https://doi.org/10.26599/FRICT.2026.9441274

Research Article

A novel superlubricity DLC/MoS_2-Ag coating and its low friction mechanism in wide temperature range

Yongqiang Fu [1], Zongjie Han [1], Dongzhou Jia [2], Feng Guo [1] *, Changsong Liu [1], Changyang Feng [1], Jiarong Wang [3], Xiaoqiang Wu [4], Xiaoxue Li [4], Ping Yang [5]

[1] School of Mechanical and Automotive Engineering, Qingdao University of Technology, Qingdao 266520, China

[2] College of Mechanical Engineering and Automation, Liaoning University of Technology, Jinzhou 121001, China

[3] Linyi Kaiyuan Bearing Co., Ltd., Linyi 276300, China

[4] College of Mechanical and Traffic Engineering, Ordos Institute of Technology, Eerduoshi 017000, China

[5] Department of Mechanical and Electrical Engineering，Yantai Automobile Engineering Professional College, Yantai 265599, China

* Feng Guo: mefguo@qut.edu.cn

Received: March 27, 2026; Revised: May 10, 2026; Accepted: May 22, 2026

© The Author(s) 2026.

Just Accepted

Abstract

To achieve reliable self-lubrication of machine components working under conditions of extreme low temperature, a carbon-based nanocomposite coating co-doped with molybdenum disulfide (MoS_2) and silver (Ag) was fabricated by high-power pulsed magnetron sputtering (HiPIMS). The microstructure, mechanical properties and tribological behaviors over wide temperature range were investigated. The results show the hardness and elastic modulus of DLC/MoS_2-Ag coating increase as the temperature decreases. At room temperature (RT) to -40°C, the coating demonstrates stable superlubricity in N_2 atmosphere with a low the coefficient of friction **(**COF) of 0.0075. This superlubricity is primarily attributed to the graphitization induced by friction and the "ordered Ag nanoparticle array" formed within the transfer film. As the temperature decreases from -40°C to -120°C, COF gradually increases to 0.0865, and the wear gradually increases. This degradation is closely related to the suppressed graphitization of the DLC coating and the deterioration of the low-friction "ordered Ag nanoparticle array" structure at interface. When the temperature is further reduced to -160°C, the graphitization of the coating is significantly inhibited, and the cryogenic mechanical performance is deteriorated, resulting in excessive consumption of Ag on the surface of the coating, which makes it difficult to maintain the special structure of the ordered Ag nanoparticle array at the friction interface. Consequently, the self-lubrication capability of the interface is further reduced, however the coating still presents COF below 0.1. These test results show that the DLC/MoS_2-Ag composite coating designed in the present study can give ultra-low COF in a wide temperature range, which provides valuable insights into the design of carbon-based coatings in extreme low temperature conditions.

Key words: DLC/MoS_2-Ag; Cryogenic mechanical properties; Cryogenic tribology; Superlubricity.

Just Accepted

1. Introduction

In aerospace, deep-space exploration, and controllable nuclear fusion, components are frequently exposed to high–low temperature cycling and cryogenic environments. Oil lubrication tends to fail owing to increased oil viscosity under such environments, whereas solid lubrication has exhibited unique advantages. For solid lubricating coatings, the tribological properties of relative-moving friction pairs at ultra-low temperatures depend on the stability of the transfer film and the mechanical properties of the coating material [1–3]. A durable and stable low-shear-stress transfer film is critical for low and stable friction under ultra-low-temperature conditions.

Solid lubricating coatings suitable for ultra-low-temperature environments can be classified into four categories: polymer coatings (e.g., PTFE) [4], soft metal coatings (e.g., Cu and Au) [5], layered dichalcogenide coatings (e.g., WS_2 and MoS_2) [6], and diamond-like carbon (DLC) coatings [7–9]. PTFE typically forms a transfer film on the counterpart surface, enabling PTFE–PTFE sliding and excellent lubrication. However, its tribological performance at low temperatures exhibits strong temperature dependence, and the formation of transfer films becomes difficult at cryogenic temperatures. The friction mechanism was governed by the physical-mechanical properties of the counterpart and the coating itself, which remained incompletely understood [4]. Soft metal coatings such as Ag can prevent direct contact between mating surfaces, reduce the interfacial shear strength, and form transfer films to achieve self-lubrication during sliding. Nevertheless, as reported by Luo [10], the COF reached approximately 0.35 at −100°C, the coefficient is too high and failed to lubricate. For MoS_2 coatings, the temperature effect on tribological behavior is atmosphere-dependent. In inert or vacuum environments, the COF shows weak temperature dependence and excellent lubrication is achieved. In oxidizing environments, decreasing temperature increased the COF and shortened the service life. For ultra-low-temperature

Just Accepted

applications, the large internal stress caused by poor thermal expansion matching between the coating and the substrate must be addressed to avoid premature coating failure [11,12].

DLC coatings shows great application potential owing to their outstanding self-lubricating performance and wear resistance. At room temperature, DLC coatings can realize a stable ultra-low COF of 0.002 under variable atmospheres. The well-accepted self-lubrication mechanisms included passivation of surface carbon dangling bonds, friction-induced graphitization, and the formation of low-shear-stress transfer films [13]. However, pure DLC coatings suffered from high internal stress and high brittleness. Especially the coating toughness is further reduced at extreme low temperatures, making the coating prone to brittle spallation and lubrication failure, which severely limited its practical application. Accordingly, elemental doping has been widely adopted to optimize the performance of DLC coatings. Studies have demonstrated that dopant elements significantly affected the overall properties of the coatings [14–17]. MoS_2/DLC composite films achieved low friction by suppressing the columnar growth of MoS_2, forming a dense composite structure, and generating friction-induced graphitized transfer films in atmospheric environments [18]. Under dry friction, DLC–Ag coatings with tailored graphite/silver (Gr/Ag) area ratios on the sputtering target can induce nanostructures with grain sizes below 10 nm and promoted the formation of sp^3 carbon bonds, thereby reducing the COF significantly from 0.72 to 0.25 and realizing ultra-low friction [19]. Some researchers have found that Si- and W-doped DLC coatings improved structural stability and load capacity by stabilizing the carbon network and forming hard phases, respectively [20–22]. While fluorine doping breaks the three-dimensional cross-linked network of sp^3-hybridized carbon atoms in DLC and generates weak C–F bonds, thus reducing film adhesion. In contrast, when Ag is doped into DLC, nano-Ag particles diffused toward the friction interface under cyclic shear stress and frictional heat during sliding, forming an Ag-rich graphitic transfer film and thereby enhancing

Just Accepted

the tribological properties of DLC coatings [25–27].

Until now, several studies have investigated the tribological properties of DLC coatings at low temperatures. The initial surface roughness has been identified as a key factor influencing the COF. As roughness increases from 0.05 μm to 0.1 μm, the COF increased gradually because the solid lubrication effect of wear debris was weakened. With a further increased to 0.5 μm, wear debris filled the surface valleys and increased the real contact area, leading to a gradual decrease of the COF [13]. In addition, the influence of cryogenic environments on DLC coatings has been studied, the wear debris of DLC coatings in liquid nitrogen transferred from the counterpart to the coating surface and forms tribolayers, resulting in an overall increase in the COF, as compared with room temperature [28,29]. At low temperatures, a harder counterpart generated super-hard wear debris and intensified interfacial shearing when sliding against DLC, causing a notable rise in the COF; meanwhile, the high wear resistance of the counterpart limited the total system wear to a low level [30]. DLC coatings can achieve a COF as low as 0.05 at 10 K, demonstrating strong potential for cryogenic lubrication applications [13,31]. For MoS_2/Ag coatings, a nanostructured layered transfer film can be formed via friction-induced Ag precipitation and MoS_2 reorientation at 170 K, enabling superlubricity [32]. Furthermore, Xu et al. [33] reported that at the liquid-nitrogen temperature of 77 K, Ag/MoS_2 composite coatings promoted the precipitation of Ag nanoparticles during friction, which synergistically recombine with MoS_2 to form a dense and nanostructured layered solid lubricating transfer film on the contact surface, thus achieving ultra-low friction.

Based on the above research, co-doping DLC with MoS_2 and Ag is expected to show the favorable self-lubricating performance at wide temperature range. Therefore, a series of carbon-based coatings (DLC/MoS_2–Ag) were fabricated via HiPIMS system. The microstructure and its friction behaviors in

Just Accepted

wild temperature were studied, and the low-friction self-lubrication mechanism was systematically investigated.

2. Experimental details

2.1. Coating preparation

A 304 stainless steel substrate (30 mm in diameter and 5 mm thick) was sequentially ground with 400, 600, 800, 1000, 1200, 1500, and 2000 grit sandpapers. The working surface was then polished with 20000 grit abrasive paste to achieve a low roughness (Ra < 20 nm). Subsequent ultrasonic cleaning was performed in petroleum ether, anhydrous ethanol, and deionized water (15 min per solvent), followed by drying under nitrogen flow and vacuum storage prior to use.

The experimental samples in this study were prepared using a multifunctional high-density plasma platform (Xinbo Technology (Dongguan) Co., Ltd., China, MS0808). The schematic diagram of the equipment principle is shown in Fig. 1, which includes four magnetron power supplies. The Cr target and WC target are arranged opposite to each other, with a MoS_2 target and a graphite-silver composite target mounted on both sides respectively, after the fixation of the samples into the chamber, the system was subjected to an evacuation process, reducing the internal pressure to 5×10^{-3} Pa. Concurrently, the system temperature was configured to 180℃. Subsequently, ion etching was conducted for a duration of 0.5 h under conditions comprising a bias voltage of -300 V and an argon flow rate of 120 sccm. This process was designed to remove the surface oxide layer and its impurities. Subsequently, a DLC/MoS_2-Ag coating was prepared according to the principle illustrated in Fig. 1. Prior to depositing the DLC/MoS_2-Ag coating, transition layers of Cr and WC were deposited to enhance film adhesion. Initially, a Cr bonding layer was deposited in an Ar atmosphere under the following conditions: Ar flow rate of 130 sccm, Cr target power of 3 kW, and deposition time of 25 minutes. Subsequently, a WC intermediate

Just Accepted

layer was deposited with an Ar flow rate of 110 sccm, WC target power of 3 kW, and deposition time of 30 minutes. Following this, a gradient transition WC/C layer was formed by gradually reducing the WC target power to 0.5 kW while maintaining the Ar flow rate at 110 sccm for an additional 30 minutes, which served to alleviate interfacial stress and improve adhesion. Finally, the Ar flow rate was maintained at 110 sccm, and acetylene (C_2H_2) was introduced at a flow rate of 75 sccm as the carbon source to prepare H-DLC to prepare the top layer, which designated as S-0. Likewise, the C_2H_2 flow rate was controlled at 50, 75, and 100 sccm to prepare the series of DLC/MoS_2-Ag top layers, which named S-1, S-2, and S-3, respectively. During the top layer preparation, the MoS_2 target and a graphite-silver (C-Ag) composite target were activated with powers set at 1.8 kW and 4 kW for 60 min, respectively, to achieve co-doping with MoS_2 and Ag elements.

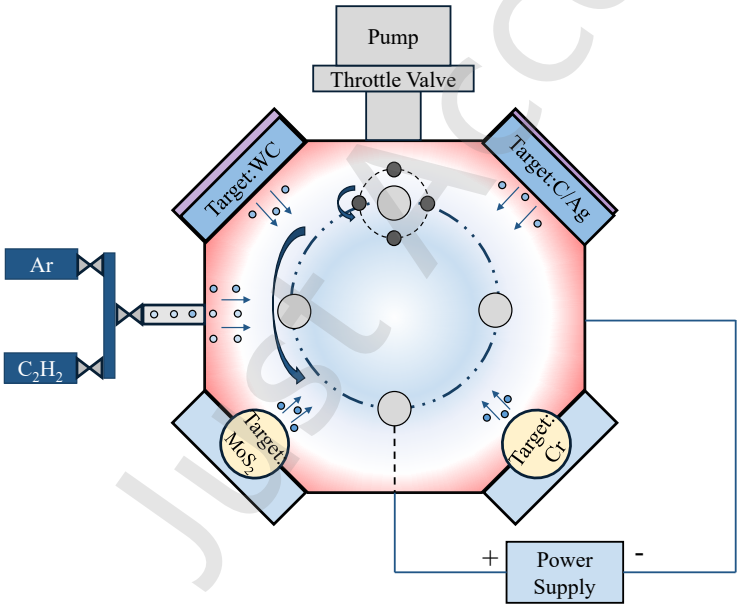


Fig 1 Multifunctional high-density plasma application platform.

2.2. Characterization

The dynamic microhardness tester (DUH-211S, Japan) was used to evaluate the hardness and elastic modulus of the coating at room temperature. The hardness tests were performed using a fixed indentation depth and loading–unloading mode. The indentation depth was set to 10% of the prepared

Just Accepted

coating thickness. A triangular pyramid indenter was employed, with an apex angle of 115° and a Poisson's ratio of 0.07. The mechanical performance at cryogenic temperature were further measured using an in-situ nanoindenter (Alemnis AG, Switzerland), the temperature was set as 0℃, -40℃, -80℃, -120℃ and -160℃. The in-situ indention video was recorded. Field-emission scanning electron microscopy (SEM, Quanta 200 FEG, Netherlands) was used to analyze the surface and cross-sectional microstructures of the coatings, with a magnification range of 10–500000. Prior to SEM observation, the coating surface was sputter-coated with gold for 30 min to improve its conductivity. The field-emission voltage was set to 5–20 kV. Additionally, the thickness of the prepared coatings was measured, and the elemental distribution and content of the coatings were qualitatively and quantitatively analyzed using an X-ray energy-dispersive spectrometer (EDS) attached to the SEM. The phase composition of the coating surface was determined using a Raman spectrometer (LabRAM HR Evolution, Horiba, France), with an excitation wavelength of 532 nm and a measurement range of 350–1200 cm^{-1}. The microstructure of the coatings was observed via transmission electron microscopy (TEM, TECNAI G2 S-TWIN F20). High-resolution transmission electron microscopy (HRTEM) and selected-area electron diffraction (SAED) were used to analyze the phase composition of the coatings. The chemical bonds and composition of the coatings were analyzed using an ESCALAB-250 X-ray photoelectron spectrometer (XPS). The Al Kα X-ray source (1468.7 eV) was operated at 164 W. During the test, the detection depth was 10 nm, and the experiment was conducted under a background vacuum of 3×10^{-8} Pa. The XPS survey scanning energy was 150 eV, and the detailed scanning energy was 20 eV. Binding energy calibration was performed using the C 1s peak at 284.8 eV. All samples were etched with Ar ions for 4 min to remove surface oxides prior to XPS testing. XPS peak deconvolution was performed using XPS4.1 software, and the test results were fitted with a Gaussian (80%) + Lorentzian (20%) function.

Just Accepted

2.3. Tribological Performance

The friction test in this paper is carried out on the ball-on-disk tribometer (MMQ-02L, Jinan Yihua Tribology Test Co., Ltd.). All the friction tests in this paper are carried out under the following conditions: (1) Temperature setting: room temperature ~ -160°C; (2) Load 2-4 N; (3) Sliding speed: 100 rpm; (4) Sliding time: 1800 s; (5) The environment is nitrogen atmosphere. The mating balls are GCr15 balls or self-mated one. After the friction test, the depth and width of the wear scar of the film are measured by a white light interferometer.

3.Results and discussion

3.1. Compositional Structure and Mechanical Properties of Films

Fig 2 (a) describes the element content of prepared coatings. As the C_2H_2 content increased, the Ag content decreased from 9.5 at.% to 5.7 at.%, the Mo and S contents decreased from 8 at.% and 15 at.% to 4.8 at.% and 8.9 at.%, respectively, and the C content increased from 67.5 at.% to 80.6 at.%. It proved that the MoS_2 and Ag have been successfully doped into the carbon-based coatings. As shown in Fig 2 ($b_1 \sim b_4$), the total thickness is controlled at 3.7~4.2 μm, the deposition efficiency was 25.5 nm/min，29.0 nm/min，27.6 nm/min，27.6 nm/min for S-0, S-1, S-2 and S-3 coatings, respectively. In Fig 2 (b_1), the prepared DLC-H coating has good density and good bonding with the transition layer, and the thickness of the top layer is about 1μm. Fig. 2 (b_5) is the TEM cross-sectional structure of the prepared DLC/MoS_2-Ag coating. The coating structure is composed of Cr transition layer, WC transition layer, WC/C transition layer and DLC/MoS_2-Ag top layer. Among them, the Cr transition layer showed a typical metal columnar growth trend, which was consistent with the previous SEM results. The WC transition layer was dense and acted as a hard layer to support the upper coating. The TEM cross-section result of top DLC/MoS_2-Ag layer also showed the compact microstructure. In addition, EDS results

Just Accepted

showed that the elements of the coating are well-distributed, which further proved that the uniformity of prepared coating. According to the Raman results in Fig 2 (c), the DLC coating showed a typical G peak at 1500-1600 cm^{-1} and a typical D peak at 1300-1400 cm^{-1} [34,35]. When MoS_2 is doped into the DLC coating, it can be found that a new peak appeared at 383~408 cm^{-1}, which corresponds to MoS_2 phase [36,37], indicating that MoS_2 has been successfully doped into the coating. The Raman signal of Ag does not appear in the coating, which is because the pure metal does not show a Raman signal peak [11]. In the Raman characterization analysis of the prepared amorphous carbon-based coatings, the D peak originates from the breathing vibration mode of sp^2-hybridized carbon, which characterizes the defects and disordered structures within the coating. The G peak corresponds to the in-plane vibration mode of sp^2-hybridized carbon atoms (stretching vibration of C–C bonds), reflecting the graphitized ordered structure of the coatings. Therefore, an increase in the I_D/I_G ratio indicates a higher proportion of defective or amorphous carbon structures relative to ordered graphite structures in the sample. In other words, a higher I_D/I_G ratio implies a lower degree of graphitization of the material, accompanied by a reduction in the content of sp^2-hybridized carbon [38,39]. According to this, it is found that the I_D/I_G ratio of the coating is significantly reduced, proving the increase of the sp^2 content of the coating due to the doping of MoS_2 and Ag into the DLC coating. When the sp^2 hybrid carbon atoms in the coating increase, the G peak will move to the high wavenumber direction. This is because the π electron cloud of the sp^2 hybrid carbon atom is more easily excited, so a stronger Raman signal will be generated [40-43]. Therefore, MoS_2 and Ag doping into the DLC coating promoted the formation and increase of sp^2 hybridization in the DLC coating. In addition, it was found that the G peak firstly shifted to the right, and then shifted to the left again with the increase of C_2H_2 flow. The ratio of I_D/I_G of the coating has experienced a process of decreasing first and then increasing. This can be explained by the fact that the sp^2 hybridization degree

Just Accepted

in the film increases first and then decreases, indicating that its graphitization degree also undergoes a process of increasing first and then decreasing. Therefore, the graphitization degree of S-2 coating is the most obvious, which also indicated that the appropriate C_2H_2 gas flow can significantly increase the graphitization of DLC. Besides, the XPS spectra of S 2p, Mo 3d, Ag 3d and C 1s of the coating were also investigated, seen in Fig. 2 (d). According to the fitting results, the peak signals of Ag 3d, Mo 3d and S 2p was detected in the DLC/MoS_2-Ag coating, indicating that Ag and MoS_2 were successfully doped into the coating. In Fig 2 (d_2-d_5), the C 1s spectrum is divided into three peaks at 284.73,285.8 and 287.9 eV, corresponding to sp2-C, sp3-C and C-O bonds, respectively [43-45]. The XPS spectra of Mo 3d fit four peaks, corresponding to $Mo^{\delta+}$ (Mo-S) at 228.5 eV and 231.7 eV [46-48], and Mo^{4+} (MoO_2) at 230.0 eV and 232.2 eV[49], respectively. The S 2p peak shows a typical characteristic peak of MoS_2, and two peaks of Ag 3d were detected at 366.7 and 372.6 eV, corresponding to Ag $3d_{5/2}$ and Ag $3d_{3/2}$, respectively [50]. The above XPS results show that the composite doping of Ag and MoS_2 is successfully doped into the DLC coating, and further proved the SEM and Raman results.

Just Accepted

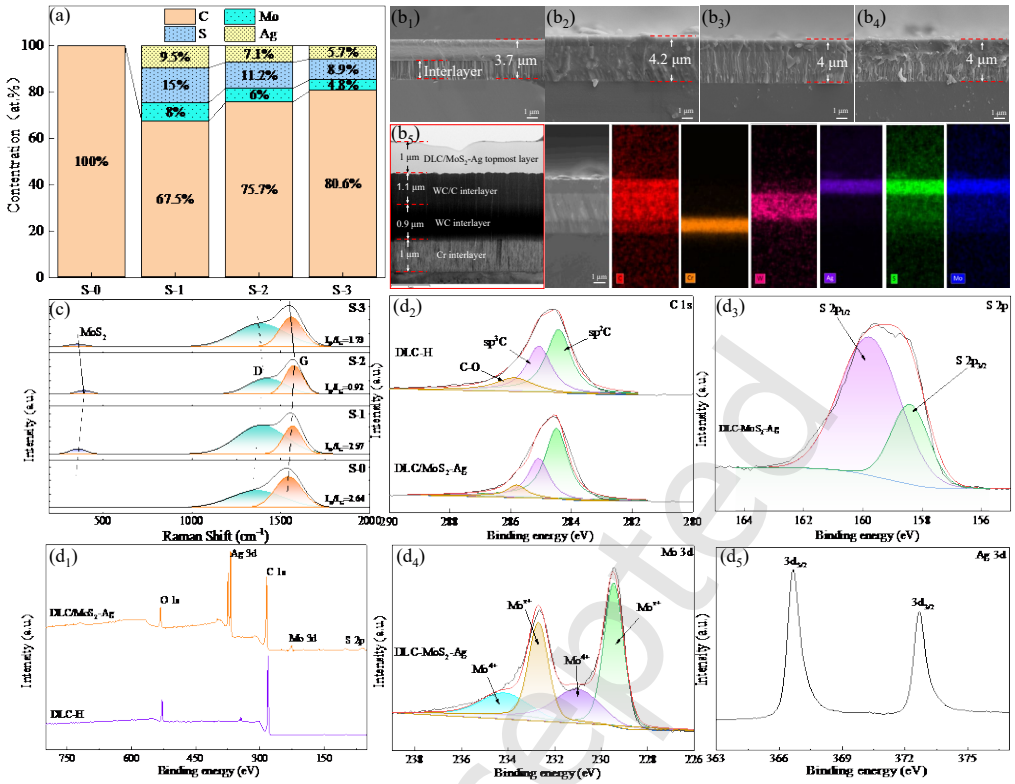


Fig 2 (a) Composition content of prepared coatings; (b_1–b_4) Cross-sectional morphologies of the prepared coatings; (b_5) TEM structure and EDS element mapping results of the S-2 coating; (c) Raman spectrum and (d) XPS results of the coating; The survey (d_1) XPS spectrum and (d_2) C 1s narrow spectrum; (d_3) S 2p narrow spectrum; (d_4) Mo 3d narrow spectrum; (d_5) Ag 3d narrow spectrum.

The adhesion strength tested by the indentation method is shown in Fig. 3(a). The indentation edge of the S-0 coating exhibited slight radial cracks and marginal peeling. This is attributed to the distortion of sp^3 hybrid bonds during the deposition of the DLC coating, which formed a complex, highly cross-linked carbon-based network with increased deformation and residual stress generation. Additionally, the mismatch in crystal structure and physical properties (thermal expansion coefficient and elastic modulus) between the DLC coating and the substrate induces stress concentration [51,52]; however, the adhesion strength still approaches the HF1 level. In contrast, the DLC/MoS_2-Ag coatings showed no radial cracks or edge peeling, demonstrating excellent adhesion with the HF1 level. This indicated that co-doping DLC

Just Accepted

with MoS_2 and Ag was beneficial for alleviating internal stress within the coating [53–56], and all the adhesion results were maintained at the HF1 level.

To further verify the adhesion test results, a WS-2005 scratch tester was used to measure the adhesion strength of the prepared coatings via the scratch method. For the scratch tests, the acoustic emission (AE) signal was used in here to evaluate the coating's adhesion. When the coating failed, the peak of the AE signal increased abruptly. However, interfering AE signals and large particles within the coating may also induce AE signal peaks. Therefore, the normal load corresponding to the AE signal peak can be used for the preliminary evaluation of the critical load [57]. As seen in Fig. 3(b), the edge of the S-0 coating peeled off under a 9 N load, with subsequent spallation intensifying. In contrast, the S-1 and S-2 coatings exhibited no peeling or substrate exposure, indicating excellent adhesion. The S-3 coating only showed slight interfacial failure. These results further proved the good adhesion of DLC/MoS_2-Ag coatings. Fig. 3(c) presents the variation of load versus indentation depth for the samples. It can be observed that both the DLC-H coating and the DLC/MoS_2-Ag coatings exhibited good elastic recovery rates, which gradually increased with increasing C_2H_2 content. In Fig. 3(d). The DLC-H coating had a hardness of 18.2 GPa and an elastic modulus of 167.2 GPa. With the addition of MoS_2 and Ag, the coating hardness decreased significantly. However, the hardness of the DLC/MoS_2-Ag coatings gradually increased from 4 GPa to 12 GPa as the C_2H_2 content increased. This variation is mainly attributed to the introduction of Ag, which significantly reduces coating hardness; the inherently low hardness of MoS_2 also synergistically decreased the overall coating hardness [56,57]. Meanwhile, the elastic modulus of the DLC/MoS_2-Ag coatings increased from 68.1 GPa to 128.7 GPa with increasing C_2H_2 content, which is also closely related to the regulation of Ag content. Fig. 3(e) shows the hard-elastic ratio of the coatings. The H/E ratio reflects the coating's ability to resist crack damage [58], while the H^3/E^2 ratio represents

Just Accepted

its resistance to plastic deformation [59]. Some research demonstrated that the crack resistance of hydrogen-free DLC coatings depended directly on their H^3/E^2 values, where coatings with higher H^3/E^2 consistently showed reduced crack lengths in nanoindentation tests and delayed crack propagation in scratch tests, proving the H/E and H^3/E^2 are meaningful values of the fracture toughness in DLC coatings [60]. So, the H/E and H^3/E^2 ratios of the S-1 coating were significantly lower than those of the DLC-H coating, proving the improvement of the fracture toughness. However, the H/E and H^3/E^2 gradually increased with the addition of MoS_2 and Ag, indicating that excessive doping reduced the mechanical properties of the coating. This may be due to the soft phase formed by Ag and MoS_2 in the coating, which decreased the total hardness of the prepared coating.

According to the above results, the indention tests have proved that the S-2 coating exhibited the favorable mechanical properties in room temperature. However, little study has been focused on the mechanical performance of DLC coating at cryogenic environment. Aiming to study the variation of mechanical performance with temperature, the S-2 coating was selected to conduct the in-situ indention test at different cryogenic temperature, and the indention behaviors was in-situ recorded as seen the attached video (it can be found in the supplemental files), it can be seen than there is no spalling or microcrack during the indention behaviors at various cryogenic temperature, and the loading-unloading curves are smooth without obvious sudden changes according to the in-situ video, indicating the favorable mechanical performance of prepared coating at such cryogenic temperatures. As seen in Fig. 3(f), it presents the variation of load with indentation depth for the sample at different temperatures. The hardness and elastic modulus of the DLC/MoS_2-Ag coating at different temperatures are displayed in Figure 3(g). At room temperature, the hardness and elastic modulus of the coating are 7.75 GPa and 84.9 GPa, respectively. With a gradual decrease in temperature, both the hardness and elastic modulus of the

Just Accepted

coating show an upward trend, reaching 12.93 GPa and 160.1 GPa at -160℃. As observed in Figure 3(h), the H/E ratio exhibits an overall decreasing trend with decreasing temperature, except for a slight increase at 0℃. The results proved that the mechanical performance of DLC coating was deteriorated. This variation was also confirmed by Zheng et al. [61], they proved that the thermal atomic motions of pure graphite were suppressed in the cryogenic temperature by using molecular dynamics, and the hardness increased. The similar phenomenon was found on the other materials, such as the metals and alloys [62,63].

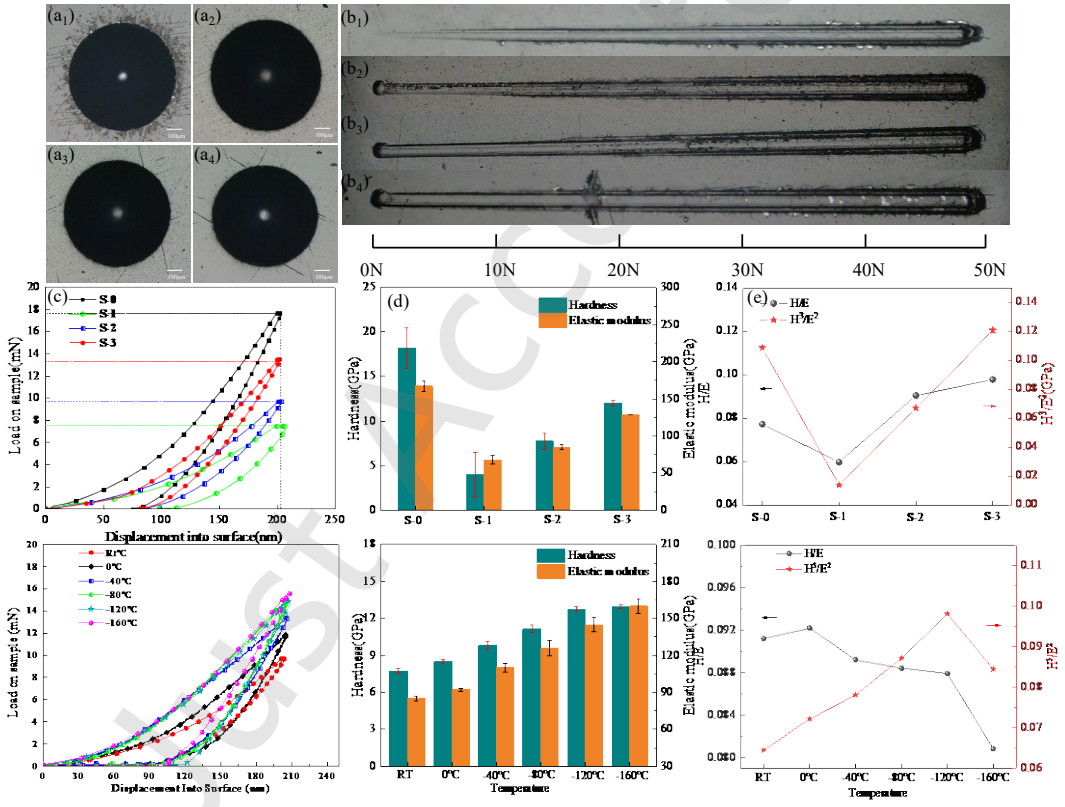


Fig 3 (a) Indention-adhesion results of: (a_1) S-0, (a_2) S-1, (a_3) S-2, (a_4) S-3; (b) Scratch-adhesion results of: (b_1) S-0, (b_2) S-1, (b_3) S-2, (b_4) S-3; Mechanical properties at RT:(c) Load-indentation depth curves; (d) Hardness and elastic modulus; (e) H/E and H^3/E^2 values; Mechanical properties at different cryogenic temperature: (f) Load-indentation depth curves; (g) Hardness and elastic modulus o; (h) H/E and H^3/E^2 values.

Just Accepted

3.2. Tribological performance under wide temperature range

To investigate the tribological properties of the DLC/MoS_2-Ag coatings, S-2 sample were selected and the tribological tests were conducted over a temperature range from room temperature (RT) to -160°C. Besides, to elaborate the contributions of MoS_2 and Ag doping to the friction behaviors at the various temperature, the friction tests of pure DLC coatings (S-0) were also conducted under the RT to -160°C. In can been seen from the Fig. S1, the COF remained stable and the ultra-low value of 0.027 at RT condition. This stable trend was broken when the temperature decreased to the -120℃. Moreover, the mean steady COF increased from the 0.027 to 0.142 for the pure DLC coating as the temperature decreased from RT to -160℃, which indicated that the cryogenic temperature inhibited the low tribological properties of the DLC coating. As shown in Fig. 4, the DLC/MoS_2-Ag coatings maintained a stable superlubricity state as the temperature range from (RT) to -40°C, all the COF were below 0.01. It achieved minimum COF of 0.0075 at 0 ℃. As the temperature decreased to -80°C, the COF of the coatings increased rapidly to 0.0515. The S-2 coating exhibited the highest COF of 0.0865 at -120°C, and then slightly decreased to 0.0785 at -160°C. All the COFs of DLC/MoS_2-Ag coating were much lower than those of pure DLC coatings, indicating the MoS_2 and Ag doping into DLC coating help to decrease the friction under the various temperatures.

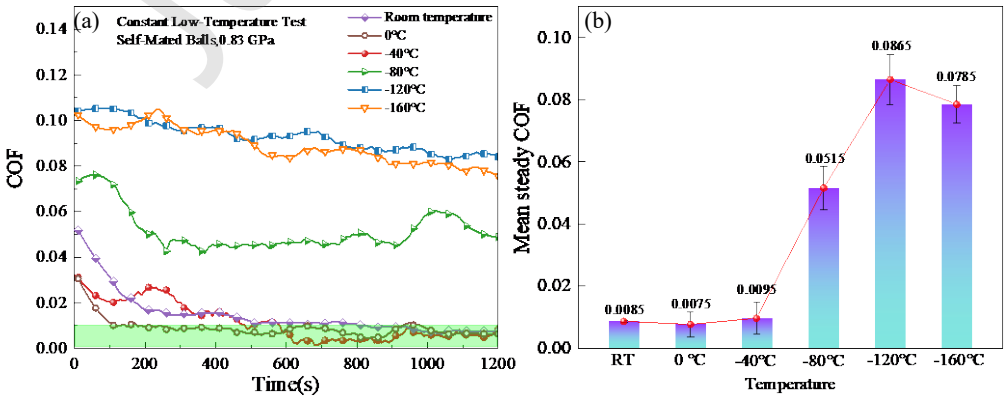


Fig. 4 Tribological properties of the S-2 coating at wide temperature range: (a) COF curves at different

Just Accepted

temperatures; (b) Mean steady COF.

To explore the wear mechanism of the coatings at cryogenic temperatures, the coating wear tracks were investigated, and it was found that the tracks were relatively flat with no obvious grooves in the temperature range of RT ~ -40°C, seen in Fig. 5(a), indicating stable tribological performance of the coatings in this temperature range. As the temperature decreased to -120°C, the depth of the coating wear tracks begins to increase and the width was getting narrow, indicating the increase of wear loss. When the temperature is reduced to -160°C, the wear scars become shallow and widen again. The upper right corner of the Fig. 5(a) shows white-light interferometry images of the wear tracks, it can be observed that the wear tracks are very slight at RT, 0°C, and -40°C, whereas the coatings at -80°C and -120°C showed clearly wear scar outlines. Raman results were analyzed to study the graphitization of the sliding interface, seen in Fig. 5(b), it presents the Raman spectra of the DLC/MoS_2-Ag coating wear tracks under different constant temperature conditions. With decreasing temperature, the I_D/I_G ratio of the wear scars gradually increases. Generally, the D-band (approximately 1350 cm^{-1}) is attributed to the stretching vibrations of sp^2-hybridized C–C bonds and C=C double bonds, while the G-band (approximately 1580 cm^{-1}) originates from the stretching vibrations of sp^2-hybridized carbon atoms and π electrons in the material [66]. The increase in the I_D/I_G ratio indicates a relative decrease in the number of sp^2-hybridized carbon atoms in the coatings, confirming that the graphitization degree at the wear track decreased with decreasing temperature. This also indicated that the formation of sp^2 of the sliding interface is limited under low-temperature conditions, leading to a reduction in the coating graphitization degree and an increase of COF. The relative increase in sp^3 content also accounted for the increase in low-temperature hardness with decreasing temperature. To further analyze the cryogenic friction mechanism, HRTEM analysis was performed on the sliding interface of pure DLC and DLC/MoS_2-Ag coatings at different

Just Accepted

temperature stages (-40°C and -160°C), as shown in Fig S2 and Figs. 5(c-h). For pure DLC coating, no obvious lattice fringes were detected inside the coating and at the sliding interface under the -40°C, which meant an amorphous phase. The sliding interfaces on the mating ball and wear debris were also amorphous. Similarly, the sliding interfaces also remained the amorphous phase for the pure DLC tribopairs under the -160°C (Fig. S2(b)). Moreover, the selected area electron diffraction (SAED) showed no obvious diffraction rings, which further proves the amorphous state of the pure DLC coating at -40°C and -160°C. This result indicated that the DLC coating relied solely on its self-lubrication and graphitization properties to maintain a low COF during the sliding process at cryogenic temperatures. Meanwhile, the decrease in temperature led to a deterioration of the mechanical properties of the coating, it can be inferred that the variation mechanical performance of pure DLC coatings caused a gradual increase of the COF. For the DLC/MoS_2-Ag coating, nano-Ag crystals dispersed in the carbon-based amorphous matrix, presenting a spherical shape with a size of approximately 5–8 nm in the coating (Fig. 5c). The lattice spacing d = 0.239 nm corresponded to the (111) crystal plane of Ag nanocrystals [28]. Notably, it was found that numerous nano-Ag crystals with the diameter of 3–5 nm were observed at the sliding interface of the DLC/MoS_2-Ag coating, and arranged in a row at the top sliding interface, and surrounded by amorphous carbon, forming a special “ordered Ag nanoparticle array” structure. On the contrary, no similar ordered structure was observed at the sliding interface on the ball surface, as shown in Fig. 5(d). In addition, the wear debris fractured by friction to form new nano-Ag clusters with the same crystal lattice Meanwhile, the new (200) crystal lattice of Ag appeared in the wear debris, with a lattice spacing of 0.205 nm. When the temperature is reduced to -160°C, the special ordered Ag nanoparticle array structure disappeared at the coating friction interface, as shown in Fig. 5(f); however, nano-Ag crystals wrapped in amorphous carbon can still be observed at a depth of 10 nm from the friction interface

Just Accepted

of the coating. In addition, no nano-Ag particles were detected on the sliding interface of the ball (Fig. 5(g)). The disappearance of this special ordered Ag nanoparticle array structure and the inhibition of coating graphitization under low-temperature conditions can explain the increase in COF at such low temperatures. In the wear debris, many numerous nano-Ag particles showed a diameter of 10–15 nm or even larger, this is can be explained by that the coating becomes brittle and hard as revealed by low-temperature mechanical testing. This leads to reduced stability of the friction interface, making the coating prone to mechanical removal. The resulting wear debris is extruded and agglomerated under contact stress, causing the original 3–5 nm Ag particles within it to reorganize into larger clusters. Meanwhile, the new Ag (200) crystal planes with a lattice spacing of 0.205 nm are detected, indicating that more Ag in the coating segregated under the ultra-low-temperature conditions, and then recombined in the wear debris under contact stress. The loss of Ag in the coating further reduced the mechanical and tribological properties. However, the overall COF of the coatings can still be maintained below 0.09 and much lower than those of DLC coatings over the temperature range from RT to -160°C, proving the contributions of MoS_2 and Ag to low friction at cryogenic temperatures.

Just Accepted

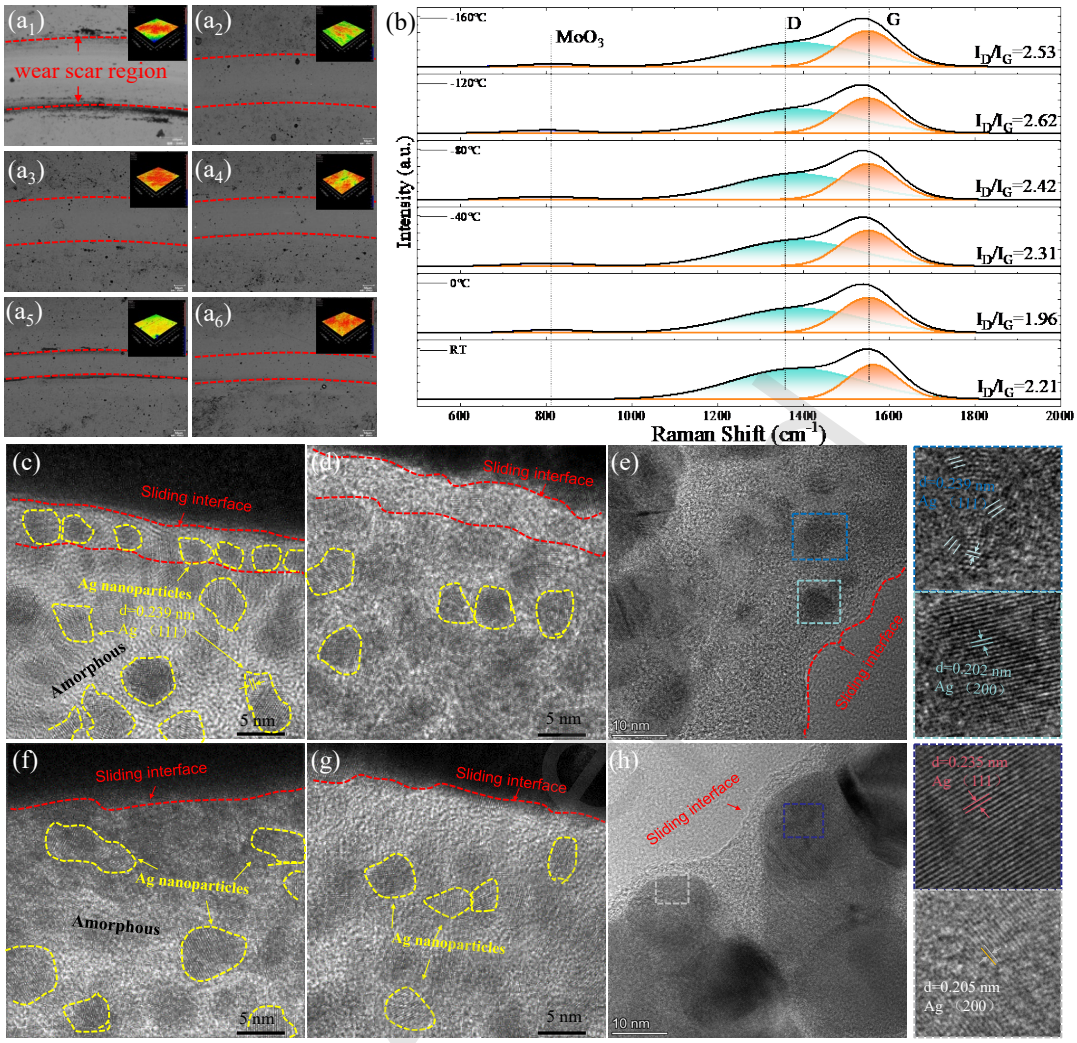


Fig. 5 (a) The wear scar optical images of DLC/MoS_2-Ag coating tribopairs under different temperature conditions : (a_1-a_6) RT, 0, -40, -80, -120 and -160°C; (b) It's corresponding Raman spectra of wear track on the prepared coating; (c-h) TEM results of the tribopairs under different temperature: The sliding interfaces of (c) coating and (d) mating ball at -40°C; (e) TEM results of wear debris at -40°C; The sliding interfaces of (f) coating and (g) mating balls at -160°C ; (h) TEM results of wear debris at -160°C;

3.3. Low-friction mechanisms of DLC/MoS_2-Ag coating under wide temperature range

Studies have shown that low temperatures can inhibit the formation of shear graphite layer and reduce the hydrogen transport rate due to the thermal activation effect [1,64], and the inhibition becomes stronger as the temperature decreases. In addition, wear and friction can consume the low-friction shear

graphite layer passivated by hydrogen at the sliding interface [1,65]. For MoS_2, the phonon-mediated energy dissipation process was frozen at low temperatures, and thermal activation was weakened, leading to the reduction of the migration ability of interlayer atoms and significantly increased interlayer shear stress [12]. Fig. 6 shows a schematic diagram illustrating the low-friction mechanism of DLC/MoS_2-Ag at different temperature. At the temperature range of RT~-40°C, the amorphous carbon matrix graphitized by the friction stress, forming a low-shear graphitic carbon layer that provides basic lubrication support for the interface. Meanwhile, Ag particles precipitates from the coatings under frictional stress, and surrounded by the amorphous carbon to form a layer of nano-silver sphere arrays at the friction interface, forming a "ordered Ag nanoparticle array" structured transfer film. It is speculated that the special structure significantly reduces interfacial friction. The self-lubrication of MoS_2 and Ag, combined with the ordered Ag array structure formed at the friction interface, constitutes a triple synergistic lubrication system, ensuring the stable superlubricity state of the coatings. Afterwards, the COF continues to increase as the ambient temperature drops below -40°C, indicating that the synergistic lubrication effect is gradually destroyed at the friction interface. This is because the I_D/I_G ratio of DLC increases significantly in a low-temperature environment, indicating that the formation of sp^2-C clusters is hindered. This inhibits the formation of the low-shear graphitic carbon layer in the transfer film, resulting in weakened lubrication at the sliding interface. Meanwhile, low temperatures lead to reduced crystallinity of MoS_2, and the loss of S elements causes deviations in the stoichiometric ratio, which further impairs its intrinsic lubrication performance. Moreover, the coatings become hard and brittle at low temperatures, and the diffusion ability of Ag atoms is reduced, making it difficult to maintain a stable " ordered Ag nanoparticle array " structure at the friction interface. Many silver particles are released and accumulated in the wear debris due to brittle fracture of the coatings, reducing the anti-friction effect of the ordered Ag

Just Accepted

nanoparticle array structure. As the temperature further decreases to -160°C, the graphitization degree of the coatings is further limited, the hardness and brittleness of the coatings continue to increase, and the mechanical properties deteriorate progressively. Most importantly, Ag particles precipitate and agglomerate in the wear debris, resulting in the complete disappearance of the " ordered Ag nanoparticle array " structure at the friction interface at -160°C, and leading to an increase in the coating COF, as shown in Fig. 6.

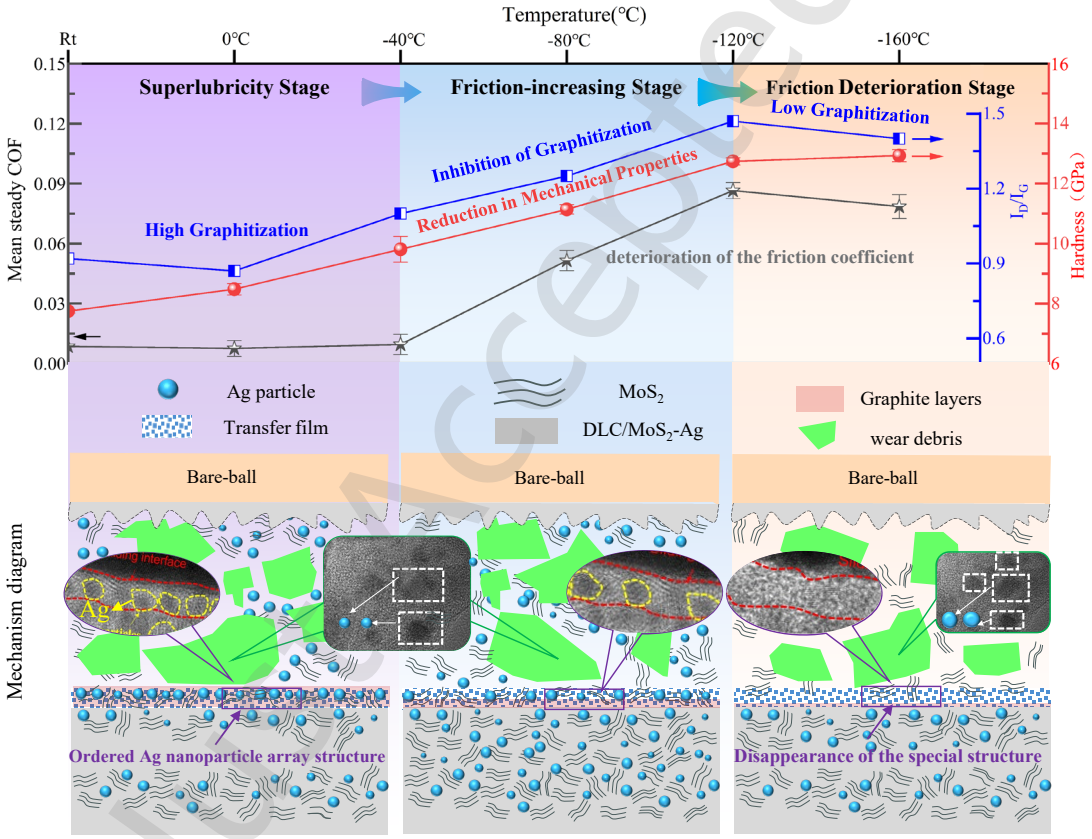


Fig 6 Schematic diagram of the low- friction mechanism of DLC/MoS_2-Ag.

4. Conclusions

1)In this paper, a series of were prepared via HiPIMS technology. The prepared coatings showed dense structure and favorable adhesion. Due to the suppression of thermal atomic motion at low temperature, the hardness and elastic modulus of DLC/MoS_2-Ag coatings increased, further leading to the increase of coating brittleness at cryogenic temperature.

Just Accepted

2) The DLC/MoS_2-Ag coatings exhibited stable superlubricity in N_2 at room temperature, with a minimum COF of 0.0075. This is attributed to the passivation of hydrogen dangling bonds on the sliding surface, the graphitization of the coatings and the special " ordered Ag nanoparticle array " structure formed by nano-Ag particles, which together constitute a superlubricity interface.

3) In the cryogenic temperature range from -40°C to -160°C, the graphitization of the coatings is inhibited, the increase of the coating brittleness and the " ordered Ag nanoparticle array " structure of nano-Ag particles is difficult to form and maintain the structure stability during the friction process. Besides. The synergistic lubrication effect weakened, causing the COF increase. However, all the COF remains below 0.09, and the prepared DLC/MoS_2-Ag coatings demonstrate excellent wide-temperature-range low-friction behavior.

Just Accepted

Acknowledgements

This work has been supported by Shandong Provincial National Natural Science Foundation Youth Project (ZR2024QE047), Shandong Province Higher Education Institutions Youth Innovation Team Project (2023KJ116), Qingdao Postdoctoral Research Project Foundation (QDBSH20240201003).

Reference

1. Aggleton M, Burton J, Taborek P. Cryogenic vacuum tribology of diamond and diamond-like carbon films. J Appl Phys, 2009, 106(1): 013504.
2. Zhao X, Phillpot SR, Sawyer WG, et al. Transition from thermal to athermal friction under cryogenic conditions. Phys Rev Lett, 2009, 102(18): 186102.
3. Wang K, Zhang J, Ma T, et al. Unraveling the friction evolution mechanism of diamond-like carbon film during nanoscale running-in process toward superlubricity. Small, 2021, 17(1): 2005607.
4. Ren Y, Zhang L, Xie G, et al. A review on tribology of polymer composite coatings. Friction, 2021, 9: 429-470.
5. Luo RR, Li PY, Zhang T, Dan M, Jin FY. Tribological and wear properties of silver solid lubricating coatings at low temperatures. Lubr Eng, 2018, 43(11): 114-119.

6. Li J, Liu R, Chu X, et al. Enhanced formaldehyde sensing performance of $CdFe_2O_4$ via surface sensitization with MoS_2 or WS_2 nanosheets. Appl Surf Sci, 2026, 731: 166389.
7. Jang S, Chen Z, Kim S H. Origin of superlubricity of diamond-like carbon (DLC). Friction, 2025, 13(1): 85-99.
8. Shi P, Sun J, Liu Y, et al. Running-in behavior of a H-DLC/Al_2O_3 pair at the nanoscale[J]. Friction, 2021, 9(6): 1464-1473.
9. One-step method to enhance biotribological properties and biocompatibility of DLC coating by ion beam irradiation. Friction, 2022(007): 010.
10. Luo R, Li P, Zhang T, et al. Tribological properties of silver solid lubricating coatings at low temperatures. Lubrication Engineering, 2018, 43(11): 114-119.
11. Yang JF, Jiang Y, Hardell J, et al. Influence of service temperature on tribological characteristics of self-lubricant coatings: a Review. Front Mater Sci, 2013, 7(1): 28-39.
12. Gradt T, Schneider T. Tribological performance of MoS_2 coatings in various environments. Lubricants, 2016, 4(3): 32.
13. Gamuly GD. Friction behaviour and wear resistance of diamond-like carbon films under cryogenic temperatures. Diamond Relat Mater, 1994, 3(11-12): 1381-1384.
14. Hou HM, Jia L, Wang YX, et al. Mechanical response and tribological behavior of Pb-doped DLC films: Molecular dynamics and first-principles study. Appl Surf Sci, 2026, 718: 164913.
15. Cheng Q, Wang G, Huang G, et al. Friction and wear reduction in PVDF by DLC coating: Interfacial mechanisms from simulation and experiment validation. Appl Surf Sci, 2026, 733: 166615.
16. Jin CY, Zhang ZY, Jia JL, et al. Comparative study of mechanical properties and tribological behavior of Si-DLC and B-DLC films. Vacuum, 2026, 248: 115215.
17. Feng F, Yang L, Yao X, et al. The Anti-Friction Mechanism of Si-DLC Films by Water Molecules: A ReaxFF Molecular Dynamics Study. Lubrication Science, 2026, 38(3): 151-162.
18. Zhu M, Liu L, Li Z, et al. Dry cutting performance and sustainability evaluation of micro-textured and DLC/MoS_2 coated ceramic self-lubricating tools. J Manuf Process, 2026, 157: 15-26.
19. Lungu CP. Nanostructure influence on DLC-Ag tribological coatings. Surf Coat Technol, 2005, 200: 198-202.
20. Zhang Y, Zhang Y, Li L, et al. Effect of alternating hydrostatic pressure (AHP) on the corrosion and tribocorrosion behavior of gradient W-DLC coated WC-based cermet. Corros Sci, 2025, 256: 113190.
21. Feng X, Cao S, Zheng Y, et al. Influence of W contents on the microstructure and tribological properties of W-DLC coatings deposited by PECVD combined with magnetron sputtering. Vacuum, 2024, 226: 113293.
22. Hu Y, Wang S, Chai L, et al. Effect of power on the microstructure and frictional properties of Si-DLC films prepared by high-power impulse magnetron sputtering (HiPIMS). Surf Coat Technol, 2025, 513: 132513.
23. Liu R, Zhang X, Lu Y, et al. Influence of laser processing parameters on wettability of F-DLC coating. Mater Today Commun, 2025, 48: 113447.
24. Zhou C, Ru L, Xiao J, et al. Cr content regulates the friction and corrosion resistance of

Just Accepted

Cr/F-DLC thin films. Diamond Relat Mater, 2025, 157: 112482.
25. Yaremchuk I, Tamulevičienė A, Tamulevičius T, et al. Optical Properties of DLC-Ag Nanocomposite and Grating Structures on their Base. Appl Mech Mater, 2014, 490-491: 53-57.
26. Buathong S, Harnchana V, Pimsawat A, et al. Electrodeposition of Ag-doped diamond-like carbon films on stainless steel for supercapacitor applications. J Alloys Compd, 2025, 1010: 177942.
27. Narayan JR, Wang H, Tiwari A. Nanostructured DLC-Ag Composites for Biomedical Applications. MRS Proc, 2002, 750(1): Y5.9.
28. Iwasa Y. Cryotribology of diamond and graphite. Cryogenics, 1996, 37(12): 801-805.
29. Presnyakova GN, Lyubarskii IM, Hubner W, et al. Friction and wear at low temperatures. Metal Sci Heat Treat, 1971, 13(3): 186-188.
30. Ostrovskaya YL. Friction and wear behaviour of hard and superhard coatings at cryogenic temperatures. Tribol Int, 2001, 34(4): 255-263.
31. Tao Y, Miao J, Jin Z, et al. Microstructure, mechanical properties and low-temperature tribological behavior of Cr/Cr-W/W-DLC/DLC multilayer coatings on 5A06 Al alloy. J Mater Res Technol, 2022, 18: 810-819.
32. Yin X, Jin J, Chen X, et al. A New Pathway for Superlubricity in a Multilayered MoS_2–Ag Film under Cryogenic Environment. Nano Lett, 2021, 21(24): 10165-10171.
33. Xu H, Cai M, Zhou H, et al. Preparation and tribological properties of Ag/MoS_2 composite coatings at liquid nitrogen temperature. Tribol Int, 2021, 163: 107187.
34. Khun N W, Liu E. Tribological properties of platinum/ruthenium/nitrogen doped diamond-like carbon thin films deposited with different negative substrate biases. Friction, 2014, 2(4): 317-329.
35. Liu M, Xu Z, Yuktanan N, et al. Scratch-induced damage of doped DLC and MoS_2 coatings—Deep symbolic analysis. Friction, 2026, 14(3): 9441166.
36. Tan CK, Wong WC, Ng SM, et al. Raman studies of MoS_2 under strain at different uniaxial directions. Vacuum, 2018, 153: 274-276.
37. Obrien M, Scheuschner N, Maultzsch J, et al. Raman spectroscopy of suspended MoS_2. Phys Status Solidi B, 2017, 254(11): 1700218.
38. Chen Z, Wei X, Lu S, et al. Surface in-situ graphitization and properties of amorphous carbon film induced by laser irradiation. Friction, 2025, 6: 167-178..
39. De Mello J D B. Carbon-based solid lubricants: An overview. Friction, 2025, 13(1): 9441017.
40. Li LH, Zhang HQ, Sun Y. Comparative analysis of DLC film fine structure by Raman spectra and X-ray photoelectron spectroscopy. Acta Phys Sin, 2001, 50(8): 1549-1554.
41. Yang WJ, Sekino T, Shim KB, et al. Microstructure and tribological properties of SiO_x/DLC films grown by PECVD. Surf Coat Technol, 2005, 194(1): 128-135.
42. Nakamura T, Tsuchiya T, Ohana T. Fabrication of sulfur-functionalized DLC films by photochemical modification and attachment of gold nanoparticles. Appl Surf Sci, 2014, 317: 443-448.
43. Wu Z, Zhou F, Wang Q, et al. Influence of trimethylsilane flow on the microstructure, mechanical and tribological properties of CrSiCN coatings in water lubrication. Appl Surf Sci, 2015, 355: 516-530.
Just Accepted

44. Erdemir A, Eryilmaz O. Achieving superlubricity in DLC films by controlling bulk, surface, and tribochemistry. Friction 2014, 2: 140–155.
45. Zhou F, Adachi K, Kato K. Influence of deposition parameters on surface roughness and mechanical properties of boron carbon nitride coatings synthesized by ion beam assisted deposition. Thin Solid Films, 2006, 497(1-2): 210-217.
46. Zhang M, Zhou F, Wang Q. Structural and tribological properties of CrMoCN coatings with various Mo contents in artificial seawater. Appl Surf Sci, 2019, 493: 485-496.
47. Chen LM, Zhang ZJ. Novel [111] oriented Mo2N thin films deposited by magnetron sputtering as an anode for aqueous micro-supercapacitors. Electrochim Acta, 2017, 245: 237-248.
48. Gusieva K, Cwalina KL, Blades WH. Repassivation Behavior of Individual Grain Facets on Dilute Ni–Cr and Ni–Cr–Mo Alloys in Acidified Chloride Solution. J Phys Chem C, 2018, 122(34): 19499-19513.
49. Feng K, Zhang Y, Li Z. Corrosion properties of laser cladded CrCoNi medium entropy alloy coating. Surf Coat Technol, 2020, 397: 126004.
50. Zhidkov IS, Kurmaev EZ, Condorelli M, Cholakh SO, Urso LD. X-ray photoelectron spectra of Ag-Au colloidal nanoparticles after interaction with linear carbon chains. Appl Sci, 2021, 11(2): 685.
51. Yong Q, Wang H, Xu B, Ma G. Research status on friction mechanism of diamond-like carbon films and influencing factors of their tribological properties. J Mech Eng, 2016, 52(11): 13.
52. Zeng Q, Cao Q, Eedemir A, et al. Research progress on ultra-low friction behavior of diamond-like carbon films. China Surface Engineering, 2018, 31(4): 7-25.
53. Wu Y, Li H, Ji L, et al. A long-lifetime MoS_2/a-C:H nanoscale multilayer film with extremely low internal stress. Surf Coat Technol, 2013, 236(24): 438-443.
54. Jiang A, Cao X, Wang Z, et al. Friction performance and corrosion resistance of MoS2/DLC composite films deposited by magnetron sputtering. Results Phys, 2021, 25: 104278.
55. Wang DY, Chang CL, Ho WY. Microstructure analysis of MoS_2 deposited on diamond-like carbon films for wear improvement. Surf Coat Technol, 1999, 111: 123-127.
56. Niakan H, Zhang C, Yang L, et al. Structure and properties of DLC–MoS_2 thin films synthesized by BTIBD method. J Phys Chem Solids, 2014, 75(12): 1289-1294.
57. Fu Y, Zhou F, Zhang M, Zhou ZF. Structural, mechanical and tribocorrosion performances of CrMoSiN coatings with various Mo contents in artificial seawater. Appl Surf Sci, 2020, 525: 146629.
58. Niu Y, Wei J, Yu Z. Microstructure and tribological behavior of multilayered CrN coating by arc ion plating. Surf Coat Technol, 2015, 275: 332-340.
59. Fu Y, Zhou F, Wang Q, Zhou ZF. The influence of Mo target current on the microstructure, mechanical and tribological properties of CrMoSiCN coatings in artificial seawater. J Alloys Compd, 2019, 791: 800-813.
60. Li H, Liu L, Guo P, et al. Long-term tribocorrosion resistance and failure tolerance of multilayer carbon-based coatings[J]. Friction, 2022, 10(10): 1707-1721
61. Zheng C, Hirayama T, Yamashita N, et al. Underlying Mechanisms of Improved Cryogenic Tribological Performance of the Pure Graphite: Suppressed Thermal Atomic Motions and Enhanced Mechanical Properties. J Tribol, 2025, 147(12): 122101.

Just Accepted

62. Ahzhan MFA, Muttaqie T, Prabowo AR, et al. A procedural and technical experimental review on material tensile and impact properties under cryogenic temperatures. E3S Web Conf, 2024, 563: 02034.
63. Mekonnin AS, Wacławiak K. Investigation of material properties under cryogenic conditions: a review. Zeszyty Nauk Organ Zarządzaj Politech Śląsk, 2025, in press.
64. Yang WJ, Niihara K, Auh KH. Microstructural characteristics and film properties of diamond-like carbon coatings grown by PECVD. J Ceram Process Res, 2004, 5(3): 232-237.
65. Zhao X, Hamilton M, Sawyer WG, et al. Thermally activated friction. Tribol Lett, 2007, 27: 113-117.
66. Iwasa Y, Ashaboglu AF, Rabinowicz ER, et al. Cryotribology of diamond and graphite. Cryogenics, 1997, 37(12): 801-805.

1. Aggleton M, Burton J, Taborek P. Cryogenic vacuum tribology of diamond and diamond-like carbon films. J Appl Phys, 2009, 106(1): 013504.
2. Zhao X, Phillpot SR, Sawyer WG, et al. Transition from thermal to athermal friction under cryogenic conditions. Phys Rev Lett, 2009, 102(18): 186102.
3. Wang K, Zhang J, Ma T, et al. Unraveling the friction evolution mechanism of diamond-like carbon film during nanoscale running-in process toward superlubricity. Small, 2021, 17(1): 2005607.
4. Ren Y, Zhang L, Xie G, et al. A review on tribology of polymer composite coatings. Friction, 2021, 9: 429-470.
5. Luo RR, Li PY, Zhang T, Dan M, Jin FY. Tribological and wear properties of silver solid lubricating coatings at low temperatures. Lubr Eng, 2018, 43(11): 114-119.
6. Li J, Liu R, Chu X, et al. Enhanced formaldehyde sensing performance of $CdFe_2O_4$ via surface sensitization with MoS_2 or WS_2 nanosheets. Appl Surf Sci, 2026, 731: 166389.
7. Jang S, Chen Z, Kim S H. Origin of superlubricity of diamond-like carbon (DLC). Friction, 2025, 13(1): 85-99.
8. Shi P, Sun J, Liu Y, et al. Running-in behavior of a H-DLC/Al_2O_3 pair at the nanoscale[J]. Friction, 2021, 9(6): 1464-1473.
9. One-step method to enhance biotribological properties and biocompatibility of DLC coating by ion beam irradiation. Friction, 2022(007): 010.
10. Luo R, Li P, Zhang T, et al. Tribological properties of silver solid lubricating coatings at low temperatures. Lubrication Engineering, 2018, 43(11): 114-119.
11. Yang JF, Jiang Y, Hardell J, et al. Influence of service temperature on tribological characteristics of self-lubricant coatings: a Review. Front Mater Sci, 2013, 7(1): 28-39.
12. Gradt T, Schneider T. Tribological performance of MoS_2 coatings in various environments. Lubricants, 2016, 4(3): 32.
13. Gamuly GD. Friction behaviour and wear resistance of diamond-like carbon films under cryogenic temperatures. Diamond Relat Mater, 1994, 3(11-12): 1381-1384.
14. Hou HM, Jia L, Wang YX, et al. Mechanical response and tribological behavior of Pb-doped DLC films: Molecular dynamics and first-principles study. Appl Surf Sci, 2026, 718: 164913.
15. Cheng Q, Wang G, Huang G, et al. Friction and wear reduction in PVDF by DLC coating:

Just Accepted

Interfacial mechanisms from simulation and experiment validation. Appl Surf Sci, 2026, 733: 166615.
16. Jin CY, Zhang ZY, Jia JL, et al. Comparative study of mechanical properties and tribological behavior of Si-DLC and B-DLC films. Vacuum, 2026, 248: 115215.
17. Feng F, Yang L, Yao X, et al. The Anti-Friction Mechanism of Si-DLC Films by Water Molecules: A ReaxFF Molecular Dynamics Study. Lubrication Science, 2026, 38(3): 151-162.
18. Zhu M, Liu L, Li Z, et al. Dry cutting performance and sustainability evaluation of micro-textured and DLC/MoS_2 coated ceramic self-lubricating tools. J Manuf Process, 2026, 157: 15-26.
19. Lungu CP. Nanostructure influence on DLC-Ag tribological coatings. Surf Coat Technol, 2005, 200: 198-202.
20. Zhang Y, Zhang Y, Li L, et al. Effect of alternating hydrostatic pressure (AHP) on the corrosion and tribocorrosion behavior of gradient W-DLC coated WC-based cermet. Corros Sci, 2025, 256: 113190.
21. Feng X, Cao S, Zheng Y, et al. Influence of W contents on the microstructure and tribological properties of W-DLC coatings deposited by PECVD combined with magnetron sputtering. Vacuum, 2024, 226: 113293.
22. Hu Y, Wang S, Chai L, et al. Effect of power on the microstructure and frictional properties of Si-DLC films prepared by high-power impulse magnetron sputtering (HiPIMS). Surf Coat Technol, 2025, 513: 132513.
23. Liu R, Zhang X, Lu Y, et al. Influence of laser processing parameters on wettability of F-DLC coating. Mater Today Commun, 2025, 48: 113447.
24. Zhou C, Ru L, Xiao J, et al. Cr content regulates the friction and corrosion resistance of Cr/F-DLC thin films. Diamond Relat Mater, 2025, 157: 112482.
25. Yaremchuk I, Tamulevičienė A, Tamulevičius T, et al. Optical Properties of DLC-Ag Nanocomposite and Grating Structures on their Base. Appl Mech Mater, 2014, 490-491: 53-57.
26. Buathong S, Harnchana V, Pimsawat A, et al. Electrodeposition of Ag-doped diamond-like carbon films on stainless steel for supercapacitor applications. J Alloys Compd, 2025, 1010: 177942.
27. Narayan JR, Wang H, Tiwari A. Nanostructured DLC-Ag Composites for Biomedical Applications. MRS Proc, 2002, 750(1): Y5.9.
28. Iwasa Y. Cryotribology of diamond and graphite. Cryogenics, 1996, 37(12): 801-805.
29. Presnyakova GN, Lyubarskii IM, Hubner W, et al. Friction and wear at low temperatures. Metal Sci Heat Treat, 1971, 13(3): 186-188.
30. Ostrovskaya YL. Friction and wear behaviour of hard and superhard coatings at cryogenic temperatures. Tribol Int, 2001, 34(4): 255-263.
31. Tao Y, Miao J, Jin Z, et al. Microstructure, mechanical properties and low-temperature tribological behavior of Cr/Cr-W/W-DLC/DLC multilayer coatings on 5A06 Al alloy. J Mater Res Technol, 2022, 18: 810-819.
32. Yin X, Jin J, Chen X, et al. A New Pathway for Superlubricity in a Multilayered MoS_2–Ag Film under Cryogenic Environment. Nano Lett, 2021, 21(24): 10165-10171.
33. Xu H, Cai M, Zhou H, et al. Preparation and tribological properties of Ag/MoS_2 composite

Just Accepted

coatings at liquid nitrogen temperature. Tribol Int, 2021, 163: 107187.
34. Khun N W, Liu E. Tribological properties of platinum/ruthenium/nitrogen doped diamond-like carbon thin films deposited with different negative substrate biases. Friction, 2014, 2(4): 317-329.
35. Liu M, Xu Z, Yuktanan N, et al. Scratch-induced damage of doped DLC and MoS_2 coatings—Deep symbolic analysis. Friction, 2026, 14(3): 9441166.
36. Tan CK, Wong WC, Ng SM, et al. Raman studies of MoS_2 under strain at different uniaxial directions. Vacuum, 2018, 153: 274-276.
37. Obrien M, Scheuschner N, Maultzsch J, et al. Raman spectroscopy of suspended MoS_2. Phys Status Solidi B, 2017, 254(11): 1700218.
38. Chen Z, Wei X, Lu S, et al. Surface in-situ graphitization and properties of amorphous carbon film induced by laser irradiation. Friction, 2025, 6: 167-178..
39. De Mello J D B. Carbon-based solid lubricants: An overview. Friction, 2025, 13(1): 9441017.
40. Li LH, Zhang HQ, Sun Y. Comparative analysis of DLC film fine structure by Raman spectra and X-ray photoelectron spectroscopy. Acta Phys Sin, 2001, 50(8): 1549-1554.
41. Yang WJ, Sekino T, Shim KB, et al. Microstructure and tribological properties of SiO_x/DLC films grown by PECVD. Surf Coat Technol, 2005, 194(1): 128-135.
42. Nakamura T, Tsuchiya T, Ohana T. Fabrication of sulfur-functionalized DLC films by photochemical modification and attachment of gold nanoparticles. Appl Surf Sci, 2014, 317: 443-448.
43. Wu Z, Zhou F, Wang Q, et al. Influence of trimethylsilane flow on the microstructure, mechanical and tribological properties of CrSiCN coatings in water lubrication. Appl Surf Sci, 2015, 355: 516-530.
44. Erdemir A, Eryilmaz O. Achieving superlubricity in DLC films by controlling bulk, surface, and tribochemistry. Friction 2014, 2: 140–155.
45. Zhou F, Adachi K, Kato K. Influence of deposition parameters on surface roughness and mechanical properties of boron carbon nitride coatings synthesized by ion beam assisted deposition. Thin Solid Films, 2006, 497(1-2): 210-217.
46. Zhang M, Zhou F, Wang Q. Structural and tribological properties of CrMoCN coatings with various Mo contents in artificial seawater. Appl Surf Sci, 2019, 493: 485-496.
47. Chen LM, Zhang ZJ. Novel [111] oriented Mo2N thin films deposited by magnetron sputtering as an anode for aqueous micro-supercapacitors. Electrochim Acta, 2017, 245: 237-248.
48. Gusieva K, Cwalina KL, Blades WH. Repassivation Behavior of Individual Grain Facets on Dilute Ni–Cr and Ni–Cr–Mo Alloys in Acidified Chloride Solution. J Phys Chem C, 2018, 122(34): 19499-19513.
49. Feng K, Zhang Y, Li Z. Corrosion properties of laser cladded CrCoNi medium entropy alloy coating. Surf Coat Technol, 2020, 397: 126004.
50. Zhidkov IS, Kurmaev EZ, Condorelli M, Cholakh SO, Urso LD. X-ray photoelectron spectra of Ag-Au colloidal nanoparticles after interaction with linear carbon chains. Appl Sci, 2021, 11(2): 685.
51. Yong Q, Wang H, Xu B, Ma G. Research status on friction mechanism of diamond-like carbon films and influencing factors of their tribological properties. J Mech Eng, 2016,
Just Accepted

52(11): 13.
52. Zeng Q, Cao Q, Eedemir A, et al. Research progress on ultra-low friction behavior of diamond-like carbon films. China Surface Engineering, 2018, 31(4): 7-25.
53. Wu Y, Li H, Ji L, et al. A long-lifetime MoS_2/a-C:H nanoscale multilayer film with extremely low internal stress. Surf Coat Technol, 2013, 236(24): 438-443.
54. Jiang A, Cao X, Wang Z, et al. Friction performance and corrosion resistance of MoS2/DLC composite films deposited by magnetron sputtering. Results Phys, 2021, 25: 104278.
55. Wang DY, Chang CL, Ho WY. Microstructure analysis of MoS_2 deposited on diamond-like carbon films for wear improvement. Surf Coat Technol, 1999, 111: 123-127.
56. Niakan H, Zhang C, Yang L, et al. Structure and properties of DLC–MoS_2 thin films synthesized by BTIBD method. J Phys Chem Solids, 2014, 75(12): 1289-1294.
57. Fu Y, Zhou F, Zhang M, Zhou ZF. Structural, mechanical and tribocorrosion performances of CrMoSiN coatings with various Mo contents in artificial seawater. Appl Surf Sci, 2020, 525: 146629.
58. Niu Y, Wei J, Yu Z. Microstructure and tribological behavior of multilayered CrN coating by arc ion plating. Surf Coat Technol, 2015, 275: 332-340.
59. Fu Y, Zhou F, Wang Q, Zhou ZF. The influence of Mo target current on the microstructure, mechanical and tribological properties of CrMoSiCN coatings in artificial seawater. J Alloys Compd, 2019, 791: 800-813.
60. Li H, Liu L, Guo P, et al. Long-term tribocorrosion resistance and failure tolerance of multilayer carbon-based coatings[J]. Friction, 2022, 10(10): 1707-1721
61. Zheng C, Hirayama T, Yamashita N, et al. Underlying Mechanisms of Improved Cryogenic Tribological Performance of the Pure Graphite: Suppressed Thermal Atomic Motions and Enhanced Mechanical Properties. J Tribol, 2025, 147(12): 122101.
62. Ahzhan MFA, Muttaqie T, Prabowo AR, et al. A procedural and technical experimental review on material tensile and impact properties under cryogenic temperatures. E3S Web Conf, 2024, 563: 02034.
63. Mekonnin AS, Wacławiak K. Investigation of material properties under cryogenic conditions: a review. Zeszyty Nauk Organ Zarządzaj Politech Śląsk, 2025, in press.
64. Yang WJ, Niihara K, Auh KH. Microstructural characteristics and film properties of diamond-like carbon coatings grown by PECVD. J Ceram Process Res, 2004, 5(3): 232-237.
65. Zhao X, Hamilton M, Sawyer WG, et al. Thermally activated friction. Tribol Lett, 2007, 27: 113-117.
66. Iwasa Y, Ashaboglu AF, Rabinowicz ER, et al. Cryotribology of diamond and graphite. Cryogenics, 1997, 37(12): 801-805.

Just Accepted



Yongqiang Fu is an associate professor, from School of Mechanical and Automotive Engineering, Qingdao University of Technology, China. His major research interests include tribology and electrochemistry of hard coatings, design and application of carbon based solid lubrication coatings, and solid–liquid combined lubrication.



Feng Guo received his B.Sc. and M.Sc. degrees from the Qingdao Institute of Architecture and Engineering, China, in 1991 and 1998, respectively. He received his Ph.D. degree from City University of Hong Kong, Hong Kong, China, in 2003. He is now a chair professor in mechanical engineering at Qingdao University of Technology, China. His research areas include numerical calculations and experiments on film lubrication, optical measurements of lubricating film thickness at the submicro/nanoscale, instrumentation development, and advanced industrial lubrication techniques.

Just Accepted